Evaporation dynamics from Ag doped He Droplets upon laser excitation

Curtis F. Jones[1], Charles Bernando[2,3], Swetha Erukala[1] and Andrey F. Vilesov[1,2*]

[1] Department of Chemistry, University of Southern California, Los Angeles, California 90089, USA
[2] Department of Physics and Astronomy, University of Southern California, Los Angeles, California 90089, USA
[3] Present address: OVO (PT. Visionet Internasional), Lippo Kuningan 20th floor, JI. HR Rasuna Said Kav. B-12, Setiabudi, Jakarta, 12940, Indonesia

Author to whom correspondence should be addressed. Electronic address: vilesov@usc.edu.

May 16, 2019

Abstract

Silver clusters were assembled in helium droplets of different sizes ranging from 10^4 to 10^{11} atoms. The clusters were heated upon laser irradiation at 355 nm and evaporation dynamics of He atoms were studied by quadrupole mass spectroscopy using signals from He^+, He_2^+ and He_4^+ splitter ions. We found that for droplets containing less than 10^7 atoms the laser irradiation leads to evaporation of He atoms. On the other hand, the laser irradiation leads to the breakup of the large droplets into smaller ones.

1. Introduction

For about three decades, He droplets served as an ultracold matrix for spectroscopic interrogation of single molecules, radicals, and ionic species. [1,2,3,4,5,6,7,8,9,10] Low temperatures of ~0.4 K in combination with the weak interaction of dopants with the homogeneous quantum liquid environment resulted in very narrow spectral lines. In addition, clusters can be readily prepared inside droplets upon sequential capture of single atoms and molecules. Availability of the large droplets containing up to 10^{11} He atoms, enabled the assembly of large molecular and metallic clusters containing up to millions of particles.[4,11] Spectroscopic measurements typically rely on the evaporation of the sizable fraction of the droplet upon absorption of the laser radiation by the dopants. The decrease of the average droplet size is often detected via the reduction of ionization efficiency of the droplets upon electron impact. So far, however, there are no reports on the evaporation dynamics following energy transfer from excited dopants to the surrounding liquid He. For the experimentally relevant droplet sizes, calculations yielded an evaporation cooling time less than about 1 μs.[11] However, such calculations were based on the possibly unrealistic assumption, that during evaporative cooling a droplet can be characterized by some equilibrium temperature, which remains constant throughout the droplet.

Metallic dopants, such as silver clusters, present a unique opportunity to study laser induced heating of the host droplets.[12] They have a large absorption cross section due to plasmon resonance, which enables one to pump sufficient energy within a few nanosecond time interval to evaporate the entire droplet. On the other hand, metal clusters are characterized by very fast electron-phonon relaxation, [13,14] which ensures the pumped electronic energy turns into heat during the laser pulse. In the case of fast equilibration within the He droplet, its peak temperature could exceed the

superfluid transition temperature of 2.17 K, which may be desirable for different experiments. On the other hand, the rate of energy transfer from the hot metal clusters to its He surrounding may present a bottleneck due to transient formation of a bubble around the cluster, as discussed previously.[12]

In this work, an attempt is made to gain insight into the mechanism of the heat transfer from embedded silver clusters to helium droplets by studying evaporation dynamics of He atoms from droplets of different sizes following laser excitation. For this purpose, the kinetics of the splitter ions such as He^+, He_2^+ and He_4^+ produced upon continuous electron beam ionization has been evaluated. The amount of ions produced is proportional to the number of electron impacts, which in turn scales with the geometric cross section of the large droplets. This is the foundation of numerous spectroscopic experiments [1,2,,4,5] where the evaporative depletion of the droplet size upon the absorption of laser radiation by dopants leads to decrease of the intensity of the He_n^+ ions after electron impact ionization. The experiments described in this paper aimed to study the dynamics of the evaporative cooling and depletion of the droplet size in large droplets a short time after the laser pulse. Whereas the He^+ ions can stem either from the ionization of the evaporated atoms or via direct ejection from the droplet, in the case of He_2^+ and He_4^+ ions only the latter mechanism is applicable. We obtained that in smaller droplets containing less than about 10^7 atoms, the laser excitation induces a transient increase in the He^+ signal and simultaneous stepwise drop in the He_2^+ and He_4^+ signals. This behavior is expected for an evaporative cooling within less than 10 μs following the laser pulse. Surprisingly, laser excitation of the doped larger droplets of about 10^{10} atoms induces a transient increase of signals from all splitter ions. We concluded that this behavior is inconsistent with simple evaporative cooling and suggests a fission of the larger droplets into a large number of smaller droplets upon the laser excitation.

2. Experimental

The molecular beam apparatus used for the experiment is described in Refs. [11, 15]. Helium nanodroplets are produced via free jet expansion of high purity He gas at a pressure of 20 bar into a vacuum through 5 μm diameter nozzle. Droplets of initial average size $\langle N_{He} \rangle_0 = 5 \times 10^4$, 1×10^7 and 1.3×10^{11} are produced at nozzle temperatures T_0 = 10 K, 7 K, and 5 K respectively. [4, 11, 16] The droplets then pick up atomic Ag in heated alumina oven containing metallic silver.[17] Further downstream the droplets are detected by an Extrel MAX300 quadrupole mass spectrometer (QMS) in a separate UHV chamber. The QMS has an upper mass range of 300 amu. The entrance aperture of the QMS, which defined the detectable solid angle of the beam, was 5 mm in diameter. The output signal from the QMS is amplified using a current preamplifier from Stanford Research Systems (SR570) usually operating at a gain of 10^6 V/A with a 5 μs nominal time constant and recorded using a National Instrument fast digitizer (PCI- MIO-16E-4) set to the minimum dwell time of 2 μs/channel.

The average number of captured Ag atoms $\langle N_{Ag} \rangle$ was estimated using attenuation of helium droplet beam as described in Ref [15]. Upon capture of each Ag, about 4000 He atoms evaporate leading to a decrease in the average droplet size which is reflected as a decline in the pressure rise ΔP_{He} in the detection chamber .[16] $\langle N_{Ag} \rangle$ can be obtained as

$$\langle N_{Ag} \rangle = \frac{\Delta P_{He}}{P_{He}} \cdot \langle N_{He} \rangle \cdot \frac{E_{He}}{E_{Ag}}$$

where E_{He} = 0.76 meV is the evaporation enthalpy of He atoms at T = 0.65 K [18], E_{Ag} is the binding energy of Ag atom to an existing Ag cluster. $E_{Ag} \approx$ 2eV for N_{Ag} up to several tens of atoms[19] and the bulk cohesive energy $E_{Ag} \approx$ 3eV for particles with $N_{Ag} \geq 10^2$. [20] In this work, a constant attenuation of $\Delta P_{He}/ P_{He} \approx 0.7$ was used to ensure maximum flux of the embedded atoms.

The absorption spectra of Ag clusters measured previously[20] shows a maximum at 355 nm which is close to the surface plasmon resonance of silver spherical clusters. Moreover, the absorption cross section per atom at 355 nm remains constant with respect to the number of atoms within a factor of two.[12,20] Henceforth, in the present work the measurements were done at 355 nm using a third harmonic of the Nd:YAG pumped by a diode laser (EKSPLA NT242). The laser produces 7 ns pulses having energy of about 0.5 mJ as measured on the He droplet beam path. The laser pulse repetition rate was set at 50 Hz. The laser beam was collimated to have a size of about 2-3 mm over the path length inside the vacuum apparatus. However, no attempts were made to make a more quantitative laser beam characterization. The laser beam was directed anti collinear to the doped droplet beam: the beams overlap over the length of about 1 m. During the 7 ns laser pulse, Ag_N cluster absorbs multiple photons.[20] Fast relaxation of the absorbed energy results in evaporation of a sizable fraction of the host He droplet. In the present work, the time evolution of the QMS signal from He^+, He_2^+ and He_4^+ ions at masses of M = 4, 8 and 16 were monitored, further designated as I_4, I_8, and I_{16}, respectively.

3. Results

Figure 1a exemplifies signals collected for droplets with average size of $\langle N_{He} \rangle \approx 4 \times 10^6$ doped with Ag atoms at $\langle N_{Ag} \rangle \approx$ 2500. The time profile of the depletion signal as measured at mass M=8 (I_8) following laser excitation has been discussed previously.[11] The laser arrives at t =

0. The signal at shortest delay times of up to about 0.1 ms corresponds to the excitation of the droplets inside or very close to the ionizer and appears at the far left of the figure. At longer delay times, the signal corresponds to droplets excited at different distances from the ionizer, with the delay time giving the corresponding time of flight of the droplets from the excitation point to the ionizer. The depletion increases at longer times because the helium droplet beam is much narrower (~1 mm) at the pickup cell than at the ionizer (~6 mm). Since the laser beam is typically narrower (~2–3 mm) than the helium beam in the ionizer, the signal at shorter times results from the excitation of only the central part of the helium beam, whereas near the pickup cell the helium droplet and laser beams completely overlap, resulting in a more efficient excitation. The signal dips to its minimum value at around t = 5.5 ms, which approximately corresponds to the droplets time of flight from the pickup cell to the ionizer and returns abruptly to the baseline level at about t = 6 ms. We attribute the dip to the transient decrease of the average He droplet size due to laser induced evaporation of He atoms. An additional dip occurs around t = 7 ms due to the transient heating of the nozzle by the laser beam.[16] The time of flight between the laser pulse and the dip enables calculation of the velocity of the droplets to be 295 m/s, 200 m/s and 170 m/s at T_0 = 10 K, 7 K, and 5 K respectively. I_8 signal due to He_2^+ ions originates exclusively upon ionization of the droplets. On the other hand, I_4 contains some sizable constant contribution from the effusive atomic He beam and from atomic He partial pressure in the QMS chamber. Likewise, I_{16} signal may have a contribution from impurity ions such as O^+. Each signal is characterized by the magnitude of the dip and baseline signal i.e., signal in absence of laser irradiation which differ between I_4, I_8 and I_{16}. Therefore, for the sake of comparison, each signal was modified by subtracting the baseline and scaling the maximum depletion to -100%. The time profiles of scaled signals for I_4, I_8 and I_{16} from Fig. 1a are shown in Figure 1b. As discussed above, the waveform of

the signals in Figure 1b reflects the geometry of the He droplet and laser beams at different distances between the pickup cell and the QMS ionizer, the effect of which is difficult to disentangle. On the other hand, the signal at short delay times corresponds to excitation of the droplets in close proximity to the ionizer, where the overlap of the laser and droplet beams is approximately independent of the distance, thus facilitating a straightforward analysis. Studying this region is the primary focus of this work, as it enables us to gain insight into the kinetics of the heat transfer between silver cluster and helium droplets. Thus, from here, only the first millisecond of time profile of the scaled I_4, I_8 and I_{16} will be shown. The complete time profile of the signals are presented in the Supplementary Materials.

Figure 1c shows the first millisecond of the time profile of the scaled signals for I_4, I_8 and I_{16} in Fig 1b. Starting at $t \approx 20$ μs, I_4 spikes at about 50 μs followed by a gradual decrease with a shoulder at around 100 μs after which the decay continues with a smaller time constant. The spike in I_4 originates from the evaporation of He atoms from the droplet following laser excitation of the embedded Ag clusters, while the droplet is inside the QMS ionizer. The 20 μs delay in the onset of the fast signal results mainly from the ion flight time through the QMS. In contrast, starting at $t = 45$ μs, I_{16} drops abruptly, and upon some oscillation at around 100 μs decreases monotonously at larger delay times. Finally, I_8 signal shows similar but less pronounced drop at $t = 36$ μs followed by smooth dependence at longer delay times. The delay in the onset of the I_8 and I_{16} signals with respect to the leading edge of the I_4 spike corresponds to the longer extraction and flight time of the He_2^+ and He_4^+ ions in the QMS. We attribute the drop in I_8 and I_{16} to the decrease in the droplet size due to evaporation of He atoms, and concomitant decrease of the ionization cross section. In addition, the results in Fig. 1c indicate that the laser induced heating of Ag clusters leads to evaporation of He atoms and not of the small He_N clusters.

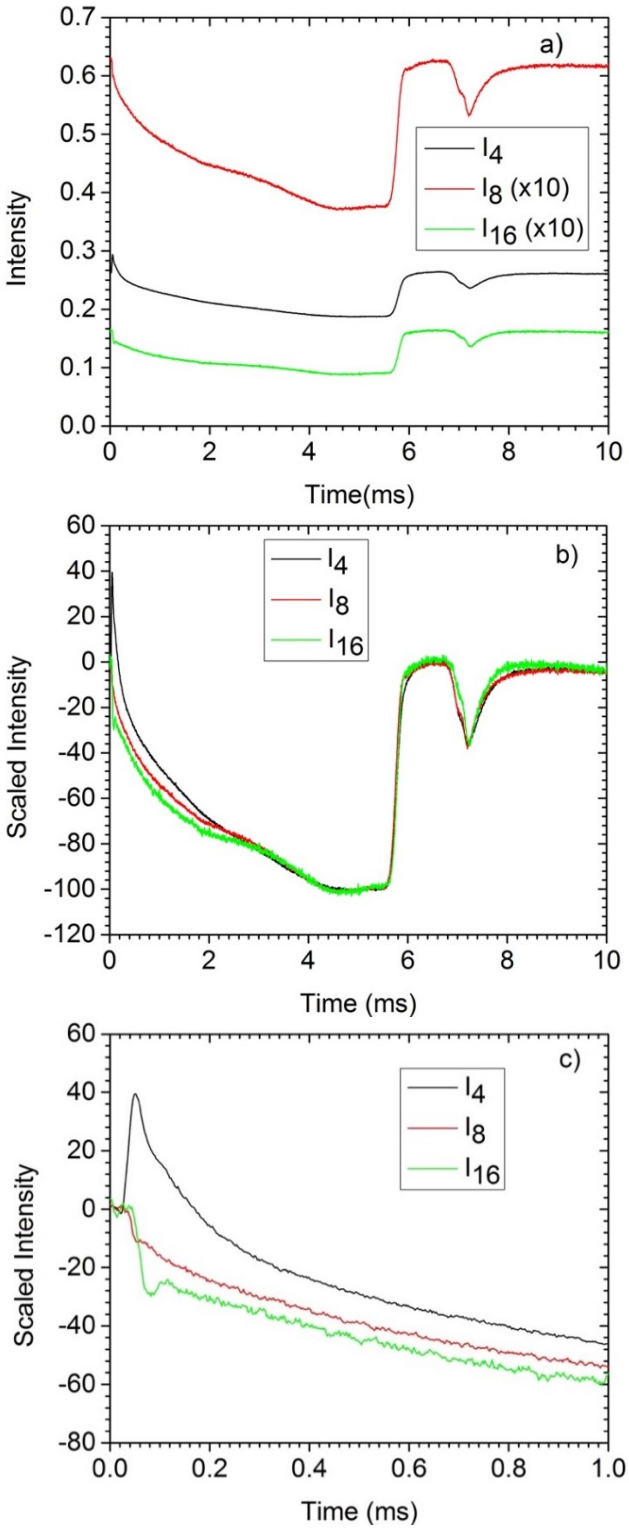

Figure 1. Time profiles of I_4, I_8 and I_{16} signals for the He droplets generated at $T_0 = 7$ K. The droplets have average size of $\langle N_{He} \rangle \approx 4 \times 10^6$ doped with Ag atoms at $\langle N_{Ag} \rangle \approx 2500$. a) Raw signal, b) signals scaled to 100% depletion for minimum dip and c) first millisecond of the scaled signal.

Figure 2a shows the results obtained upon exciting silver doped small droplets containing $\langle N_{He} \rangle = 2.5 \times 10^4$ and $\langle N_{Ag} \rangle = 5$. I_4 spikes with an onset time of 20 μs followed by a fall with ever-decreasing slope. I_8 shows a drop in the same way without a spike. The signal profiles resemble those in Figure 1c, except I_8 does not show a pronounced initial drop. The time profile for the weak I_{16} signal could not be reliably collected in small droplets because of a high noise level. Figure 2b is identical to Fig. 1c and is shown for comparison. Figure 2c shows the time profiles of I_4, I_8, and I_{16} following laser excitation of silver doped large droplets containing $\langle N_{He} \rangle = 1.5 \times 10^{11}$ and $\langle N_{Ag} \rangle = 3.4 \times 10^7$. Large droplets show distinctly different behavior at short delay times in that the signal at each mass has an early spike at delays of 50 - 100 μs. In addition, I_8 and I_{16} signals show some sharp dips at short times of 30 μs and 45 μs, respectively.

In the experiments described in Figs 2a, 2b and 2c, the signal contains a large contribution from the undepleted He droplet beam as the He droplet beam is wider than the laser beam at the ionizer. In a set of additional experiments, the central part of the He droplet beam was selected by a 400 μm diameter orifice placed along the beam axis in the differential pumping chamber ≈450 mm upstream from the ionizer. The orifice reduces the droplet flux by a factor of ≈20. Therefore, a larger preamplifier gain of 10^7 V/A had to be used, which implies a larger time constant of the amplifier of ≈50 μs. Measurements with the orifice were performed at 7 K and 5 K. The resulting time profiles are shown in Fig. 3a and 3b for the droplets with the average sizes of $\langle N_{He} \rangle \approx 4 \times 10^6$ ($\langle N_{Ag} \rangle \approx 2500$) and $\langle N_{He} \rangle = 1.5 \times 10^{11}$ ($\langle N_{Ag} \rangle = 3.4 \times 10^7$), respectively. In Fig. 3a, the time profiles at short times are similar to those in Figure 2b but the signals show larger initial rise with the orifice in place due to more effective excitation of the droplet beam which has smaller diameter and better overlap with the laser beam. Comparison of Fig. S1 C and S2 B shows that the ratio of the peak I_8 intensity to the baseline is about a factor of 7 larger in the measurements with the

orifice. Upon arrival at the QMS ionizer, the He beam expands to about 600 μm. For comparison, a factor of 6 enhancement is found in case of a Gaussian beam with 2 mm halfwidth. The signals are also smoother due to a larger time constant of the preamplifier. Likewise, the time profiles in Fig. 3b are similar to that in Figure 2c except they show a higher rise and are comparatively broader. Despite growing much larger and changing shape slightly, the different mass spikes retain the same relative magnitude with respect to each other in Fig. 2c and Fig. 3b. The fact that all signals (I_4, I_8, I_{16}) show similar short time rise indicates the change of the droplet disintegration mechanism from atom by atom evaporation to some more violent scenario.

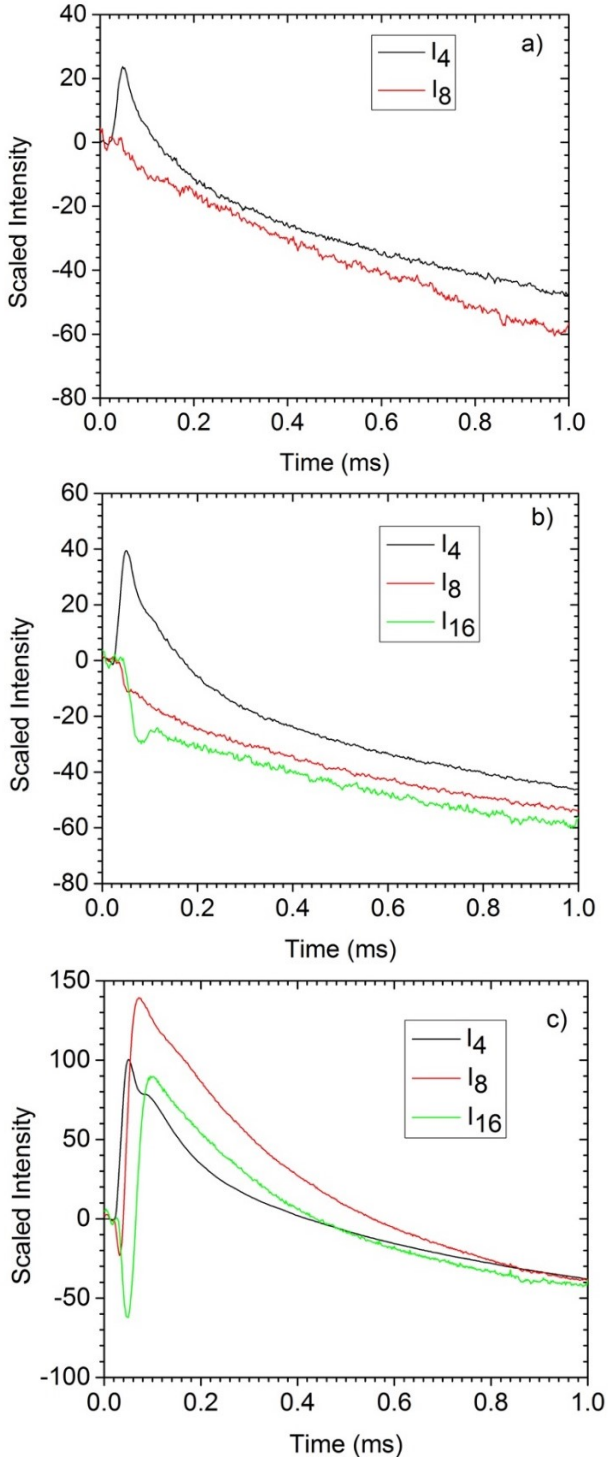

Figure 2. Time profiles of I_4, I_8 and I_{16} signals for droplets generated at nozzle temperature, T_0 = 10 K, 7 K and 5 K in panels a), b) and c), respectively. The average droplet (Ag cluster sizes) are $\langle N_{He} \rangle = 2.5 \times 10^4$ ($\langle N_{Ag} \rangle = 5$), $\langle N_{He} \rangle \approx 4 \times 10^6$ ($\langle N_{Ag} \rangle \approx 2500$) and $\langle N_{He} \rangle = 1.5 \times 10^{11}$ ($\langle N_{Ag} \rangle = 3.4 \times 10^7$), respectively.

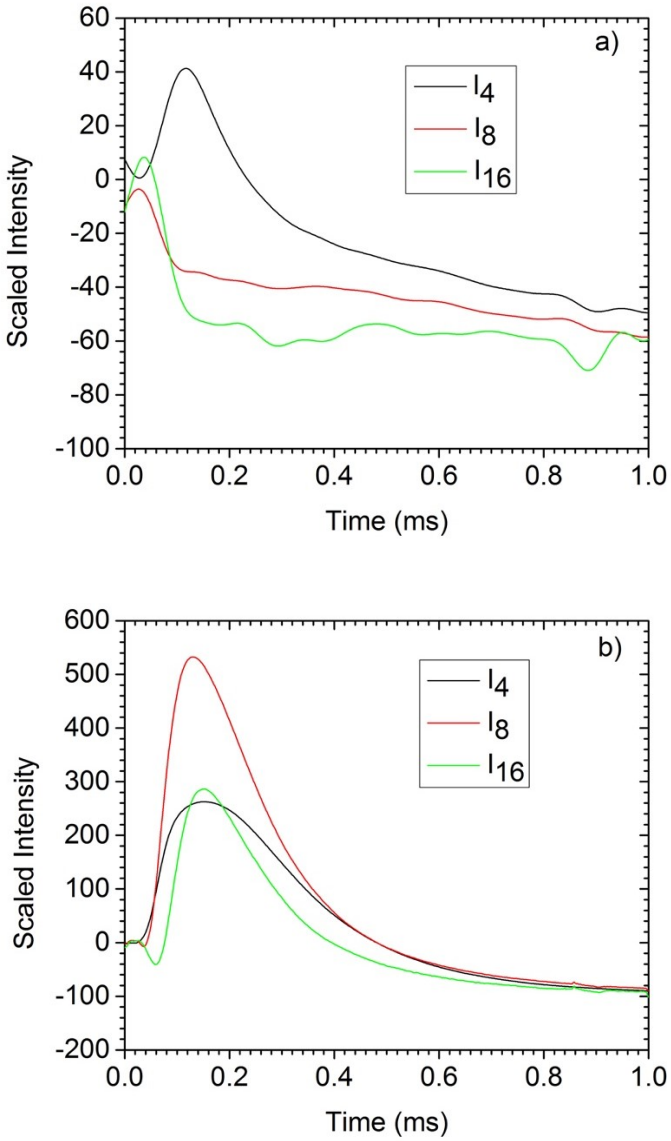

Figure 3. Time profiles of I_4, I_8 and I_{16} signals for droplets generated at nozzle temperature T_0 = 7 K and 5 K in panels a) and b), respectively. The average droplet (Ag cluster sizes) are $\langle N_{He} \rangle \approx 4 \times 10^6$ ($\langle N_{Ag} \rangle \approx 2500$) and $\langle N_{He} \rangle = 1.5 \times 10^{11}$ ($\langle N_{Ag} \rangle = 3.4 \times 10^7$), respectively. The experiments were done with 400 μm orifice placed along the beam axis.

4. Discussion

Measurements described in this work span a large range of droplet sizes (after doping) of $\langle N_{He} \rangle$ = 2.5 × 10^4, 4× 10^6 and 1.5 × 10^{11} obtained at T_0 =10 K, 7 K and 5 K, respectively. Investigation of the mass spectrum[12] shows that the relative intensities in the range of small splitter ions, which are relevant for this work, remain rather similar. He_4^+ ions present a notable exception because their intensity increases in large droplets due to different formation mechanism to be discussed later. As discussed earlier,[11,20] compact single clusters are formed in the smallest droplets upon one by one addition of Ag atoms. In the intermediate sized droplets produced at T_0 = 7 K, the aggregation is dominated by a multi-center cluster formation mechanism, where smaller clusters are formed in different locations inside the droplet, which later coagulate into a cluster-cluster aggregate. The microscopic structure of such an aggregate remains unknown, but it is useful to consider it as being composed of a collection of spherical clusters of various sizes that form a disordered aggregate. Such clusters may still possess an individual surface plasmon resonance, each of which interacts with the others, leading to the broadening and extension of the spectrum in the infrared region. Finally, multiple quantum vortices are present in the largest droplets.[21, 22] In large droplets, atoms recombine at the vortex cores faster than in the bulk of the droplet, leading to growth of filament shaped clusters.[11] The individual filaments are then aligned along the direction of the total droplet's angular momentum and are separated from each other by about 100 nm. The onset of the vortex formation in He droplets was recently studied by x-ray scattering,[23] where it was found that droplets of about 10^8 atoms contain a small number of vortices between 2 and 6. Unfortunately, smaller droplets produce insufficient x-ray scattering signal for the same measurements. However, it is reasonable to assume that the droplets of about 10^7 atoms will contain at most 1 or 2 vortices, whereas in droplets of about 10^{10} atoms, arrays containing hundreds

of vortices were observed.[21] The spectra of the Ag clusters in the droplets of different size have been discussed previously. [12] It was also argued, that the clusters may reconstruct upon pulsed laser irradiation. Absorption of laser radiation by cluster-cluster aggregates and filament shaped clusters may melt the clusters, resulting in the formation of compact, spherical clusters. Reconstruction of deposited Ag clusters at room temperature is well documented.[24]

The pulsed excitation proceeds during the 7 ns laser pulse. The plasmon excitations in Ag clusters dephase within ≈10 fs,[25] while the electron-electron and electron-phonon relaxation times are on the order of 1 ps,[13,14] both much shorter than the duration of the laser pulse. Therefore, during the laser pulse Ag cluster experiences a series of absorption – relaxation cycles. This work employed laser fluence of about 10-15 mJ/cm^2. Our earlier work[12] indicated that at these conditions the depletion signal experiences some pronounced saturation effects, which manifest in a rather similar way for different droplet/cluster sizes. The saturation effects will not influence the conclusions of this work, which are based on the observed dynamics, rather than the magnitude of the signals. The absorbed energy releases as heat within Ag clusters during the laser pulse, leading to the concomitant increase of the temperature to higher than about 1000 K[12] as estimated for the clusters excited in the center of the laser beam.

Although superfluid He is characterized by an exceptionally large heat conductivity, heat transfer from a solid to superfluid He is known to be inefficient due to a large mismatch in the velocity of sound, an effect known as Kapitza resistance.[26]Above certain critical values of the heat flux on the order of ≈1 W/cm^2,[27] a bubble of He gas will be formed which effectively insulates the hot body from the liquid He environment. This effect was dramatically manifested in early experiments in which a tungsten filament was heated while inside a vessel filled with superfluid He.[28] Recent experiments have shown the formation of bubbles in liquid He upon production of

silver alloy clusters by laser ablation.[29] Estimates[12] show that the excited silver clusters are not able to dissipate the heat during the laser pulse as the required heat transfer rate must then substantially exceed the critical value for the bubble formation. Therefore, a bubble will likely be formed around the hot Ag cluster, resulting in a slower heat release into the droplet, whose rate could not be estimated at present time. In addition, a prolonged residence of the clusters at high temperature will likely result in the melting of the odd- shaped clusters into spherical entities.

The duration of the initial fast drop of the I_8 signal immediately after the laser pulse in Fig. 1c of about 15 μs corresponds to the time during which the evaporation of He atoms from the droplet mostly proceeds. This time is comparable with the nominal 5 μs time constant of the preamplifier and presents an upper boundary for the cooling time of the Ag clusters.

The results obtained at $T_0 = 10$ and 7 K in Fig. 2a and Fig. 2b show rather similar behavior. Upon laser pulse, the I_4 signal rises to its maximum within about 15 μs, whereas I_8 signal drops sharply during about the same time. The width of the I_4 peak seems somewhat longer in larger droplets, being about 40 μs as compared with about 60 μs for droplets produced at $T_0 = 10$ K and 7 K, respectively. Both peaks show some shoulder about 20 μs past the maximum, which is more pronounced in the case of the larger clusters. We also note that the initial drop of the I_{16} signal is about twice that of I_8, which indicates different formation kinetics of the He_2^+ and He_4^+ species. The He_2^+ ions are produced upon direct ionization of the He droplets. On the other hand it was proposed that He_4^+ is formed upon collision of two metastable $He_2(a\ ^3\Sigma_u^+)$ molecules on the droplet surfaces resulting in Penning ionization followed by ejection of He_4^+.[30,31,32] Because the kinetics of the He_4^+ formation remains to be understood, in the following discussion we will use the I_8 signal as the indicator of the droplet size depletion. Here, we focus on the discussion of the results obtained in larger droplets at $T_0 = 7$ K, as they have better signal to noise ratio as compared to

smaller droplets. Moreover, the heat capacity of a large droplet is dominated by phonons and rotons, and its cooling kinetics has been modeled in Ref[11].

The initial decrease of the droplet size upon the laser pulse for the droplets in the beam center, could be estimated from the initial depletion of $\Delta I_8/I_8 = 0.2$ in Fig. SI -2a. Because the ionization efficiency of the large droplets is proportional to the geometric cross section of the droplet, the fractional decrease of the droplet size can be found as: $\Delta N/N=1.5\times\Delta I_8/I_8 = 0.3$. [16] The obtained $\Delta N/N$ can be used to estimate the temperature and enthalpy of the droplets upon absorption. Assuming an instant heating of the droplet upon the laser pulse, the initial temperature can be estimated from Fig. 8.2 in Ref.[11] to be about 4 K. The actual temperature rise will be smaller taking into account that the heat release from Ag clusters into the liquid helium environment is slower than the cooling rate due to the evaporation. From the latent heat of vaporization of liquid He which ranges from 68 to 93 J/mol at 0.4 and 2 K, respectively, [18] the heat released from the Ag clusters into the 4×10^6 He atoms droplet could be estimated to be about 10^3 eV or 0.4 eV per Ag atom in the clusters, in agreement with previous estimates of the energy absorbed by Ag clusters based on the absorption cross section.[12] These estimate show that the absorbed energy is sufficient to increase the temperature of the droplet to the level, significantly higher than the superfluid transition temperature of 2.17 K. However, the observed fall time of the I_8 signal of about 15 μs, which could be associated with the evaporation time, is likely defined by the time response of the detection system and possibly extraction time, and thus only gives an upper estimate of the evaporation time. Accordingly, the fall does not contain any features, which may be related to the bubble formation as discussed above or slower cooling in the vicinity of the superfluid transition temperature. Passing through the superfluid transition temperature is manifested as a change in the calculated evaporation rate vs time, see Fig. 8.2 in Ref[11]. Ideally, in the case of evaporation at

thermal equilibrium, the falling edge of I_8 should resemble that in the afore mentioned figure. In addition, the thermal equilibrium evaporation is expected to be much faster and proceeds on the time scale of about 100 ns in the droplets of 10^7 He atoms. In Ref[11] it was argued, that evaporative cooling is likely slower as predicted by the thermal equilibrium model, however, the present results show that it can be as slow as 15 μs. These results call for even faster measurements, which could only be achieved with a time of flight mass spectroscopy.

It is remarkable that the initial rise of the I_4 signal proceeds within the time comparable to that for the I_8 signal fall. However, the falling edge of the I_4 signal is five times slower and contains some shoulder. Some broadening of the I_4 signal with respect to the I_8 one is likely related to the fact that He_2^+ ions are produced on the axis of the ionizer, whereas the He^+ ions originate in the entire ion range, thus causing slower extraction of the latter. In addition, the shoulder in the I_4 signal may be related to the ionization of the He atoms reflected from the construction parts of the ionization cage of the QMS. All these effects result in additional broadening and shape distortion of the I_4 signal, which makes it a poor messenger for the evaporation kinetics.

The observed dynamics are remarkably different in the largest droplets ($\langle N_{He} \rangle = 1.5 \times 10^{11}$ and $\langle N_{Ag} \rangle = 3.4 \times 10^7$) obtained at $T_0 = 5$ K. This difference is possibly not the result of a laser saturation, as the saturation effect was found to be very similar for the droplets produced at 7K and 5K.[12] The I_4 signal shows similar shape as in the smaller droplets, with sharp rise within about 20 μs, and a shoulder. The I_4 peak is about a factor of 2 broader in larger droplets, which can be related to overall a factor of nearly 100 times stronger droplet beam[16] and concomitant slower pumping of the He atoms from the ionization region. However, both I_8 and I_{16} signals after some initial sharp drop, show strong positive peaks, with even larger width than that for the I_4 peak. The I_8 and I_{16} is incompatible with just an evaporation from a single large droplet. The five-fold

increase of the I_8 signal indicates correspondingly larger overall cross section for creation of the He_2^+ ions, which can for example result from the fission of the large droplets into a number of smaller droplets. The cross section for ionization and creation of He^{2+} scales as the droplet's geometric cross section or as $N_{He}^{2/3}$. Thus, upon fission of the large droplet into n smaller droplet of same size, the overall ionization cross section will increase by a factor of $n^{1/3}$. Therefore, the five-fold increase of the I_8 signal is consistent with the fission of the droplet into 125 droplets of similar size within about 20 μs upon laser excitation of the containing clusters. The fission of the droplet may be facilitated by the existence of multiple quantum vortices in large droplets, which serve as nucleation centers for multiple (up to hundreds) of well separated Ag clusters. Excitation of the clusters followed by bubble formation and expansion may tear the droplet apart, supporting the above scenario. The formation of the bubble and following fission of the droplet involve motion of large masses and may require substantial induction time. During this time the droplet will lose some of its atoms due to evaporation, similar to the case in smaller droplets. The initial drop in the both I_8 and I_{16} signals in Fig. 2 C may be caused by such initial evaporation. If correct, the time required for fission of the large droplets may be estimated to be about 20 μs.

Finally, we note that using the short (≈ 0.1 ms) positive I_4 signal as a messenger may facilitate better signal to noise ratios in spectroscopic measurements with pulsed lasers. In comparison the traditional depletion measurements[11] entail integration of the ≈6 ms long signals and often contain a noise contribution from some low frequency, which ultimately limits the sensitivity of the technique.

5. Conclusions

In this work, helium droplets containing about 10^4, 10^7 and 10^{10} He atoms were doped with a large number of silver atoms. Silver atoms coagulate inside the droplets into clusters. The doped droplets were irradiated by pulsed laser radiation at 355 nm. Absorption by silver clusters leads to an increase of the droplet temperature and concomitant evaporation of He atoms. The dynamics of evaporation were studied by quadrupole mass spectroscopy to detect the time evolution of the He^+, He_2^+ and He_4^+ ions. Upon close investigation of the short time profile of He^+, He_2^+ and He_4^+ signals it was concluded that for droplets of sizes less than about 10^7, evaporative cooling takes place within 15 μs which is slower than the thermal equilibration evaporation. The slower evaporative cooling was attributed to the slower heat release from clusters to the helium droplet due to helium bubble formation around clusters. For larger droplets of sizes of the order of 10^{10} a rise in the signals from He^+, He_2^+ and He_4^+ was observed. This behavior was attributed to the fission of large droplets into smaller droplets of similar sizes. The different behavior of evaporation dynamics between large droplets and smaller droplets is conjectured to be due to the existence of multiple quantum vortices in large droplets. Finally, we note that the time resolution in this work is limited by the time constant of the preamplifier as well as the extraction time from the QMS ionizer. Therefore, in order to unambiguously resolve the evaporation dynamics, future experiments may employ time of flight mass spectroscopy.

6. Supporting Information

Full time profile (10ms) and normalized signals of mass = 4,8,16 for droplets generated at 10 K, 7K and 5 K and for droplets generated at 7 K, 5 K with 400 μm orifice placed along the beam axis.

7. Acknowledgements

This material is based upon work supported by the National Science Foundation under Grant No. CHE-1664990.

References

1. Toennies, J. P.; Vilesov, A. F., Spectroscopy of Atoms and Molecules in Liquid Helium. *Annu. Rev. Phys. Chem.* **1998,** *49*, 1-41.
2. Callegari, C.; Lehmann, K. K.; Schmied, R.; Scoles, G., Helium Nanodroplet Isolation Rovibrational Spectroscopy: Methods and Recent Results. *J. Chem. Phys.* **2001,** *115*, 10090-10110.
3. Stienkemeier, F.; Vilesov, A. F., Electronic Spectroscopy in He Droplets. *J. Chem. Phys* **2001,** *115*, 10119-10137.
4. Toennies, J. P.; Vilesov, A. F., Superfluid Helium Droplets: A Uniquely Cold Nanomatrix for Molecules and Molecular Complexes. *Angew. Chem. Int. Ed. Engl.* **2004,** *43*, 2622-2648.
5. Choi, M. Y.; Douberly, G. E.; Falconer, T. M.; Lewis, W. K.; Lindsay, C. M.; Merritt, J. M.; Stiles, P. L.; Miller, R. E., Infrared Spectroscopy of Helium Nanodroplets: Novel Methods for Physics and Chemistry. *Int. Rev. Phys. Chem.* **2006,** *25*, 15-75.
6. Stienkemeier, F.; Lehmann, K. K., Spectroscopy and Dynamics in Helium Nanodroplets. *J. Phys. B* **2006,** *39*, R127-R166.
7. Callegari, C.; E.Ernst, W., In *Handbook of High-Resolution Spectroscopy*, Quack, M.; Merkt, F., Eds. Wiley: Chichester, UK, 2011; Vol. 3, pp 1551-1594.
8. Kuyanov-Prozument, K.; Skvortsov, D.; Slipchenko, M. N.; Sartakov, B. G.; Vilesov, A., In *Physics and Chemistry at Low Temperatures*, 2011; pp 203-230.
9. Mauracher, A.; Echt, O.; Ellis, A. M.; Yang, S.; Bohme, D. K.; Postler, J.; Kaiser, A.; Denifl, S.; Scheier, P., Cold Physics and Chemistry: Collisions, Ionization and Reactions inside Helium Nanodroplets Close to Zero K. *Phys. Rep.* **2018,** *751*, 1-90.
10. Verma, D.; Tanyag, R. M. P.; O'Connell, S. M. O.; Vilesov, A. F., Infrared Spectroscopy in Superfluid Helium Droplets. *Advances in Physics-X* **2018,** *4*, 1553569.
11. Tanyag, R. M.; Jones, C. F.; O'Connell, S.; Verma, D.; Vilesov, A. F., In *Cold Chemistry: Molecular Scattering and Reactivity near Absolute Zero* Dulieu, O.; Osterwalder, A., Eds. Royal Society of Chemistry: Cambridge: 2018; pp 389-443.
12. Gomez, L. F.; O'Connell, S. M. O.; Jones, C. F.; Kwok, J.; Vilesov, A. F., Laser-Induced Reconstruction of Ag Clusters in Helium Droplets. *J. Chem. Phys.* **2016,** *145*, 114304.
13. Voisin, C.; Del Fatti, N.; Christofilos, D.; Vallee, F., Ultrafast Electron Dynamics and Optical Nonlinearities in Metal Nanoparticles. *J. Phys. Chem. A* **2001,** *105*, 2264-2280.
14. Maillard, M.; Pileni, M. P.; Link, S.; El-Sayed, M. A., Picosecond Self-Induced Thermal Lensing, from Colloidal Silver Nanodisks. *J. Phys. Chem. B* **2004,** *108*, 11876-11876.
15. Mozhayskiy, V.; Slipchenko, M. N.; Adamchuk, V. K.; Vilesov, A. F., Use of Helium Nanodroplets for Assembly, Transport, and Surface Deposition of Large Molecular and Atomic Clusters. *J. Chem. Phys* **2007,** *127*, 094701.
16. Gomez, L. F.; Loginov, E.; Sliter, R.; Vilesov, A. F., Sizes of Large He Droplets. *J. Chem. Phys.* **2011,** *135*, 154201-154209.
17. Loginov, E.; Gomez, L. F.; Vilesov, A. F., Surface Deposition and Imaging of Large Ag Clusters Formed in Helium Droplets *J. Phys. Chem. A* **2011,** *115*, 7199-7204.
18. Donnelly, R. J.; Barenghi, C. F., The Observed Properties of Liquid Helium at the Saturated Vapor Pressure. *J. Phys. Chem. Ref. Data* **1998,** *27*, 1217-1274.
19. Kruckeberg, S.; Dietrich, G.; Lutzenkirchen, K.; Schweikhard, L.; Walther, C.; Ziegler, J., Multiple-Collision Induced Dissociation of Trapped Silver Clusters Ag_n^+ ($2 \leqslant n \leqslant 25$). *J. Chem. Phys.* **1999,** *110*, 7216-7227.

20. Loginov, E.; Gomez, L. F.; Chiang, N.; Halder, A.; Guggemos, N.; Kresin, V. V.; Vilesov, A. F., Photoabsorption of Ag_n(N ~ 6-6000) Nanoclusters Formed in Helium Droplets: Transition from Compact to Multicenter Aggregation. *Phys. Rev. Lett.* **2011,** *106*, 233401.
21. Gomez, L. F.; Ferguson, K. R.; Cryan, J. P.; Bacellar, C.; Tanyag, R. M. P.; Jones, C.; Schorb, S.; Anielski, D.; Belkacem, A.; Bernando, C.; Boll, R.; Bozek, J.; Carron, S.; Chen, G.; Delmas, T.; Englert, L.; Epp, S. W.; Erk, B.; Foucar, L.; Hartmann, R.; Hexemer, A.; Huth, M.; Kwok, J.; Leone, S. R.; Ma, J. H. S.; Maia, F.; Malmerberg, E.; Marchesini, S.; Neumark, D. M.; Poon, B.; Prell, J.; Rolles, D.; Rudek, B.; Rudenko, A.; Seifrid, M.; Siefermann, K. R.; Sturm, F. P.; Swiggers, M.; Ullrich, J.; Weise, F.; Zwart, P.; Bostedt, C.; Gessner, O.; Vilesov, A. F., Shapes and Vorticities of Superfluid Helium Nanodroplets. *Science* **2014,** *345*, 906-909.
22. Tanyag, R. M. P.; Bernando, C.; Jones, C. F.; Bacellar, C.; Ferguson, K. R.; Anielski, D.; Boll, R.; Carron, S.; Cryan, J. P.; Englert, L.; Epp, S. W.; Erk, B.; Foucar, L.; Gomez, L. F.; Hartmann, R.; Neumark, D. M.; Rolles, D.; Rudek, B.; Rudenko, A.; Siefermann, K. R.; Ullrich, J.; Weise, F.; Bostedt, C.; Gessner, O.; Vilesov, A. F., Communication: X-Ray Coherent Diffractive Imaging by Immersion in Nanodroplets. *Struct. Dyn.* **2015,** *2*, 051102.
23. Jones, C. F.; Bernando, C.; Tanyag, R. M. P.; Bacellar, C.; Ferguson, K. R.; Gomez, L. F.; Anielski, D.; Belkacem, A.; Boll, R.; Bozek, J.; Carron, S.; Cryan, J.; Englert, L.; Epp, S. W.; Erk, B.; Foucar, L.; Hartmann, R.; Neumark, D. M.; Rolles, D.; Rudenko, A.; Siefermann, K. R.; Weise, F.; Rudek, B.; Sturm, F. P.; Ullrich, J.; Bostedt, C.; Gessner, O.; Vilesov, A. F., Coupled Motion of Xe Clusters and Quantum Vortices in He Nanodroplets. *Phys. Rev. B* **2016,** *93*, 180510.
24. Schnedlitz, M.; Lasserus, M.; Knez, D.; Hauser, A. W.; Hofer, F.; Ernst, W. E., Thermally Induced Breakup of Metallic Nanowires: Experiment and Theory. *Phys. Chem. Chem. Phys.* **2017,** *19*, 9402-9408.
25. Bosbach, J.; Hendrich, C.; Stietz, F.; Vartanyan, T.; Trager, F., Ultrafast Dephasing of Surface Plasmon Excitation in Silver Nanoparticles: Influence of Particle Size, Shape, and Chemical Surrounding. *Phys. Rev. Lett.* **2002,** *89*, 257404.
26. Pollack, G. L., Kapitza Resistance. *Rev. Mod. Phys.* **1969,** *41*, 48-81.
27. Vinson, J. S.; Agee, F. J.; Manning, R. J.; Hereford, F. L., Phenomena Resulting from Heating of Small Wires in He II. *Phys. Rev.* **1968,** *168*, 180-182.
28. Spangler, G. E.; Hereford, F. L., Injection of Electrons into He II from an Immersed Tungsten Filament. *Phys. Rev. Lett.* **1968,** *20*, 1229-1230.
29. Popov, E.; Mammetkuliyev, M.; Eloranta, J., Dynamics of Vortex Assisted Metal Condensation in Superfluid Helium. *J. Chem. Phys* **2013,** *138*, 204307.
30. Buchenau, H.; Northby, J. A.; Winkler, C.; Toennies, J. P., Electron Impact Excitation and Ionization of ^{4}He Clusters. *Jpn. J. Appl .Phys.* **1987,** *26*, 11.
31. Schöbel, H.; Bartl, P.; Leidlmair, C.; Denifl, S.; Echt, O.; Märk, T. D.; Scheier, P., High-Resolution Mass Spectrometric Study of Pure Helium Droplets, and Droplets Doped with Krypton. *Eur. Phys. J. D* **2011,** *63*, 209-214.
32. Fine, J.; Verma, D.; Jones, C. F.; Wittig, C.; Vilesov, A. F., Formation of He_4^+ Via Electron Impact of Helium Droplets. *J. Chem. Phys.* **2018,** *148*, 044302.

TOC Graphic